Journal of Applied Mathematics and Physics, 2023, 11, 2491-2502
https://www.scirp.org/journal/jamp
ISSN Online: 2327-4379
ISSN Print: 2327-4352

Numerical Study on the Duct Acoustic Mode Control of Turbine Interaction Noise with Serrated Configurations

Kangshen Xiang, Weijie Chen*, Jianxin Lian, Weiyang Qiao

School of Power and Energy, Northwestern Polytechnical University, Xi'an, China
Email: *cwj@nwpu.edu.cn

How to cite this paper: Xiang, K.S., Chen, W.J., Lian, J.X. and Qiao, W.Y. (2023) Numerical Study on the Duct Acoustic Mode Control of Turbine Interaction Noise with Serrated Configurations. *Journal of Applied Mathematics and Physics*, **11**, 2491-2502.
https://doi.org/10.4236/jamp.2023.118160

Received: June 2, 2023
Accepted: August 28, 2023
Published: August 31, 2023

Abstract

Turbine noise would be one of the dominant noise sources especially in future UHBR (Ultra High Bypass-Ratio) aeroengine, but its currently far from being studied enough. Acoustic mode is crucial for duct propagation but little study about the relation between serration and mode. Thus, taking axial single-turbine test bench NPU-Turb as object, the effect of Stator with Serrated Trailing-edge (Bionic S) and Rotor with Serrated Leading-edge (Bionic R) on duct acoustic modes of turbine turbulence interaction noise were studied in detail using DDES/AA hybrid model validated by acoustic experiment of NPU-Turb. Serval conclusions can be made here. First, for broadband noise, the effect of serrations on duct modes (increased or reduced of PWL_{mn}) with the increasing frequency is more prominent. Second, the changing trend of ΔPWL_{mn} is something like Chinese character "人" with circumferential mode m and alternating with radial mode. Such distribution is more obvious at higher frequency. More theoretical and mechanistic research work needs to be carried out in depth in the future.

Keywords

Turbine Interaction Noise, Duct Acoustic Mode, NPU-Turb, Bionic S, Bionic R

1. Introduction

In the future UHBR (Ultra-High Bypass-ratio engine), turbomachinery (fan and turbine mainly) noise would become the dominant noise sources [1] [2]. Larger fan diameter and shorter nacelle would cause more serious fan noise radiation problem [3]. While the continuous attention and research on fan noise from the

past to the future will effectively solve this problem. However, such luck didn't come to turbine noise, at least not yet.

In UHBR engine, another need is for turbine with fewer blade numbers, higher loaded and smaller axial spacing, which would yield more intense tonal and broadband turbine noise [4]. This is called "turbine noise storm" problem [5]. Unfortunately, current turbine design does not undergo acoustic processing, and few lectures mean a serious lack of turbine noise prediction capabilities and control methods. As a whole, turbine noise deserves more focus.

In terms of noise control technology, bionics has received a lot of attentions in the past decades. On the one hand, different noise sources such as airfoil trailing edge noise [6] [7] [8] and fan rotor/vane interaction noise [9] [10] have been reduced with serrated leading-edge or trailing-edge; on the another hand, from the traditional sinusoidal and sawtooth type at the beginning to the combination with slits [11] [12] and porosity [13] [14] [15], many kinds of serrations have been widely studied. Considering the similar sound generation mechanism of turbomachinery, serrations for reducing turbine noise has great potential and preliminary works have been done in previous study by authors [16], however, which is far from enough.

Besides, duct acoustic mode is crucial for fan noise and turbine noise [17] [18]. If the PWL (Sound Power Level) of the "cut-on" modes at some dominant frequencies can be reduced or the modes that were before cut-on can be cut-off by some means, more gains of noise reduction will be obtained. Such idea has not been thoroughly studied and serrations may have the ability by the first way theoretically because it makes influence on the radial mode.

Based on above analysis, one problem that what the effects of serration on propagation characteristic of duct acoustic mode especially radial mode of turbine interaction noise would be answered by using DDES [19] [20]/AA [21] hybrid model. The work is further study of previous study [22] where total noise radiation variation of stator serrated trailing-edge (Bionic S) and rotor serrated leading-edge (Bionic R) with A/W = 2 compared with baseline has been preliminary compared and its mechanism has been discussed.

The results indicate that serration has the ability to control duct acoustic modes by reducing modal radiation energy. However, currently it is far from mastering such control law, which may be a great research direction.

2. DDES/AA Hybrid Model

In order to solve the conflict between computational accuracy and resource limitation, flow-field/acoustic-field hybrid calculation method was born. For wake turbulence interaction noise of turbomachinery, in order to capture enough source information, LES (Large Eddy Simulation) method is usually applied. But the demand for grid within the boundary layers is still overwhelming.

For turbine interaction noise, turbulence information of upstream wake and its interaction process with downstream blade are critical, but it doesn't matter

in boundary layers. In such case, DES-class method [18] can be useful. After the calculation of the flow field is completed, the unsteady pressure information is extracted from the source surface, and then couples with acoustic analogy equation [21] to calculate the sound propagation.

Duct aeroacoustics propagation equation with uniform moving medium was proposed by Goldstein in 1976. For interaction noise, only needing to consider dipole sources, the governing equation is as follows:

$$p(\bar{x},t)=\int_{-T}^{T}\int_{s(\tau)}\frac{\partial G}{\partial y_i}f_i ds(\bar{y})d\tau \tag{1}$$

where $\bar{y}$ represented noise coordinates. τ and t were the radiation time and receiving time respectively. $s(\bar{y})$ was the wall surface, and c_0 was sound speed. The loading on the blade surface was f_i and G represented the Green function of the solid boundary in annular duct.

$$\begin{aligned}G(\bar{y},\tau/\bar{x},t)=&\frac{i}{4\pi}\sum_{m,n}\frac{\Psi_m(\kappa_{mn}r)\Psi_m^*(\kappa_{mn}r')}{\Gamma_{mn}}\cdot\exp[im(\phi-\bar{\phi})]\\&\times\int_{-\infty}^{\infty}\{\frac{\exp[i\omega(\tau-t)]}{k_{mn}}+\frac{\exp[i\frac{Ma\cdot\omega}{\beta^2\cdot c_0}(y_1-x_1)]}{k_{mn}}\\&+\frac{\exp[i\frac{k_{mn}}{\beta^2}|y_1-x_1|]}{k_{mn}}\}d\omega\end{aligned} \tag{2}$$

where m and n were circumferential and radial modal orders in solid duct. $Ma=U/c_0$ was axial Mach number of main stream. $r=\sqrt{x_2{}^2+x_3{}^2}$, $r'=\sqrt{y_2{}^2+y_3{}^2}$, $\phi=\arctan(\frac{x_3}{x_2})$ and $\bar{\phi}=\arctan(\frac{y_3}{y_2})$. ω was frequency of interest. $k_{mn}=\sqrt{k_0{}^2+\beta^2\kappa_{mn}^2}=\sqrt{(\omega/c_0)^2+(1-Ma^2)\kappa_{mn}^2}$ in which κ_{mn} was eigenvalue of mode (m, n) and it can be solved by characteristic function Ψ_{mn}.

Equation (1) can be expressed as follows in frequency domain:

$$p(\bar{x},\omega)=\sum_m\sum_n P_{mn}(\omega)\Psi_{m,n}(\kappa_{m,n}r)\exp(im\phi-i\gamma_{m,n}x_1) \tag{3}$$

where P_{mn} was the pressure amplitude of mode (m, n). And $\gamma_{mn}=(Ma\bullet k_0\pm k_{mn})/\beta^2$, in which "+" represented upstream direction and "−" was opposite. From the expression above, it was obvious that the solve of $P_{mn}(\omega)$ was a key step to obtain the pressure fluctuation at interested frequency.

$$\begin{aligned}P_{mn}(\omega)=&\frac{1}{2i\Gamma_{mn}\kappa_{mn}}\int_{S_F}\Psi_{mn}(\kappa_{mn}r')\cdot\bar{n}(\bar{y}_0)\times\nabla[\exp(-im\phi'+i\gamma_{mn}y_1)]\\&\times[\sum_{s=0}^{V-1}P_s(\bar{y}_0,\omega-m\Omega)\exp(i2\pi ms/V)]ds(\bar{y})\end{aligned} \tag{4}$$

Then the sound power of mode (m, n) can be expressed as:

$$W_{mn}(\omega)=\frac{\pi(r_D^2-r_H^2)}{\rho_0 U}\bullet\frac{\mp Ma^2(1-Ma^2)^2(\omega/U)k_{mn}(\omega)}{[\omega/c_0\pm Mak_{mn}(\omega)]^2}\bullet[P_{mn}(\omega)\cdot(P_{mn}(\omega))^*] \tag{5}$$

where expressions and solution methods of $\Psi_{m,n}(\kappa_{m,n}r)$. The PWL at one frequency can be calculated by superposition of all modal acoustic power level at this frequency, as expressed follows:

$$W(\omega) = \sum_{m=-\infty}^{\infty} \sum_{n=0}^{\infty} w_{mn}(\omega) \tag{6}$$

Since the broadband noise is random, the calculation of the modal sound power requires the use of statistical averaging:

$$< W_{mn}(\omega) >= \frac{\pi(r_D^2 - r_H^2)}{\rho_0 U} \cdot \frac{\mp Ma^2(1-Ma^2)^2(\omega/U)k_{mn}(\omega)}{[\omega/c_0 \pm Mak_{mn}(\omega)]^2} \cdot < P_{mn}(\omega) \cdot (P_{mn}(\omega))^* > \tag{7}$$

3. Experiment Validation

3.1. Experimental Setting

Axial single-turbine test bench NPU-Turb of TAAL (Turbomachinery Aerodynamics & Acoustics Laboratory) of NPU (Northwestern Polytechnical University) is used to validate the DDES/Goldstein hybrid model.

Some basic design parameters of NPU-Turb have been given in **Table 1**. As showed in **Figure 1**, two linear and equally spaced arrays with 32 microphones were arranged 180˚ apart along the axial wall. The axial distance between two adjacent microphones is 15 mm. Behind arrays, four reference microphones are arranged at equal angles in the circumferential direction. The arrays were rotated using gears and measurements were taken every 4˚.

Table 1. Design parameters of NPU-Turb.

Parameters	Value
Rotor numbers	40
Stator numbers	30 (40)
Axial distance, mm	20
Rotor tip clearance, mm	0.425
Expansion ratio	1.08
Massflow rate, kg/s	6.3552
Rotation speed, rpm	3000

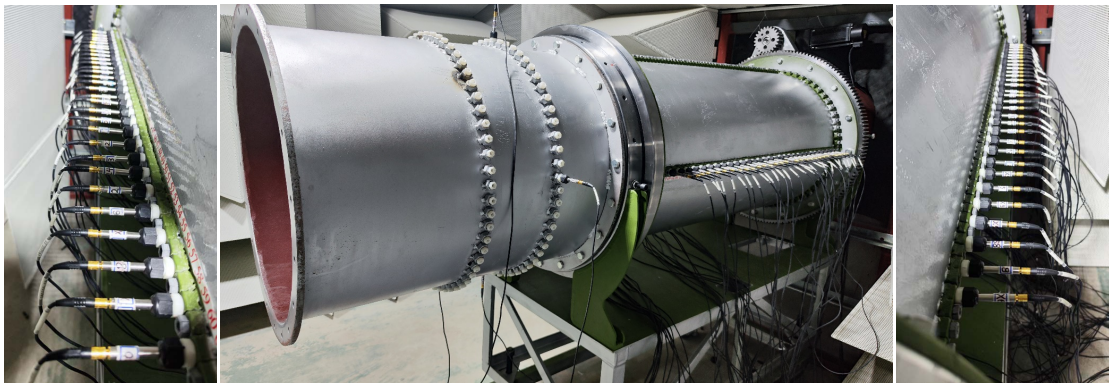

Figure 1. Experimental setting and microphone arrays.

3.2. Mesh and Computational Setting

The computational regions and mesh around blade region are given in **Figure 2**. The inlet region and outlet region were extended to avoid acoustic wave reflection. H-O-H multi-block structured grid with O-grid on the surface around the blade and H-grid in other areas was applied for baseline case with total nodes is about 27.65 million. Time discretization in second-order backward Eulerian format and spatial discretization in high-precision format were set for DDES simulation. 40 steps are calculated for a single blade channel, and the time step length is 0.00001 s at the design speed. The complete 2000 steps are run first to make the calculation converge, and then the 4000 steps are continued, corresponding to two rotation periods. The studied upper frequency is 10 KHz, and according to Nyquist's sampling theorem, a transient result can be output every 4 steps to satisfy the computational requirements.

3.3. Validation Results

Figure 3 compared the PWL of DDES/AA hybrid model with experimental data,

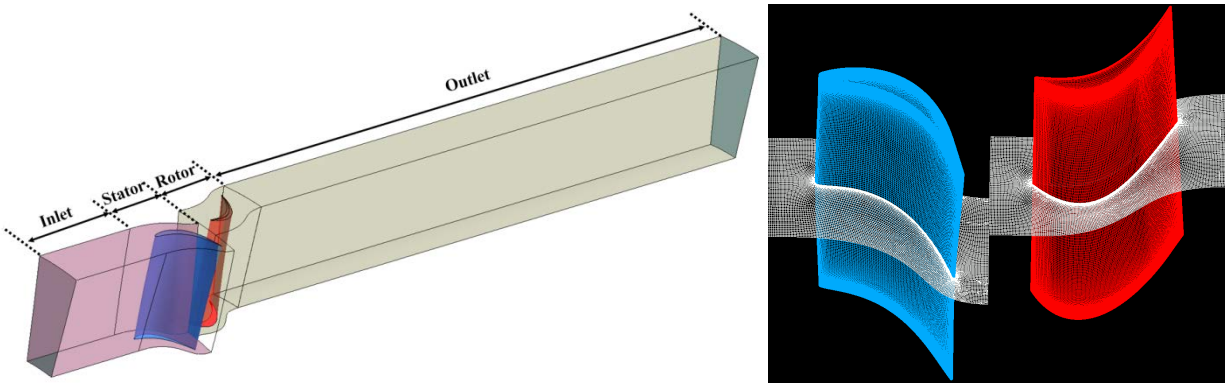

Figure 2. Computational region and mesh around blade.

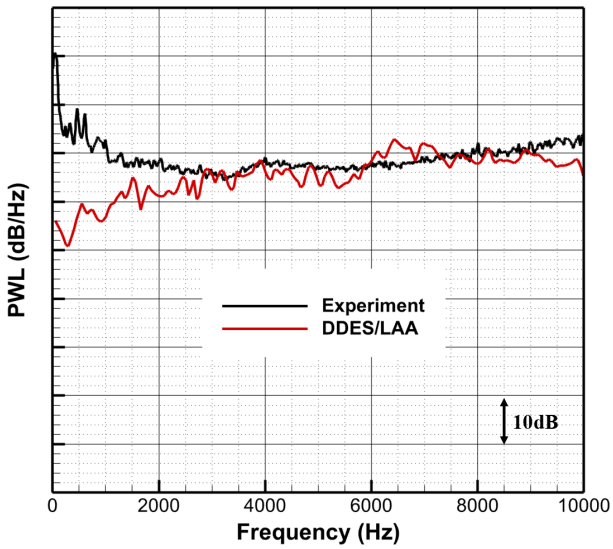

Figure 3. PWL comparation between experiment result and hybrid model prediction result.

which indicated that DDES has the ability to perform source simulation of turbine interaction noise and the mesh is sufficient.

4. Bionic Configurations

The detailed bionic blade design method and calculation cases are detailed in the [22] where the effects of Bionic S and Bionic R on duct acoustic mode have not been studied and discussed in detail which are the main contents here. The bionic configurations are showed in **Figure 4**.

5. Discussion of Duct Acoustic Mode changes with Serration

First of all, it should be noted that when performing the turbine noise prediction by DDES/Goldstein hybrid model, the Tyler criterion [17] ($m = nB \pm kV$, in which m is cut-on circumferential mode, n is harmonic number of blade passing frequency, k is arbitrary constant, B and V are rotor numbers and stator numbers respectively) is not used to judge whether the modes has been cut-on for BPFs, so only the broadband information is analyzed in detail at this time.

Figure 5 and **Figure 6** give modal sound power changes with bionic R and Bionic S from −100 to 100 of circumferential mode m below 10 KHz. The darker the color, the greater the gain. The area marked with white means increased modal sound power. In general, both Bionics S and Bionic R play good suppression for most modal sound power level.

To better analyze the effect of serrations on duct modes. **Figure 7** gives PWL changes of cut-on mode (m, n) at some certain frequencies inclding 1000 Hz, 3000 Hz, 5000 Hz, 7000 Hz, 10,000 Hz. The larger the positive value is, the more nosie reduction gains. Serval comclusions can be made here. First, for both bionic R and bionic S, the variation of the modal sound power level shows an approximately symmetrical distribution characteristic with the axial mode m. Second, for one circumferential mode m at a certain frequency, the ΔPWL_{mn} varies alternately with the radial mode n. Such characteristic is much more obvious at high frequency because more radial modes can be cut-on and the most typical one is Bionic R at 9000 Hz. Third, the influence of Both Bionic S and Bionic R on modal sound power increases with increasing frequency. Unfortunately, there is currently no way to considert the effect of serration with

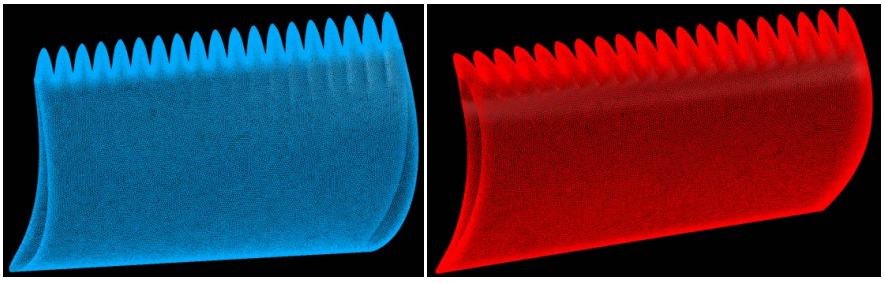

(a) (b)

Figure 4. Meshes and structures of Bionic configurations. (a) Bionic S; (b) Bionic R.

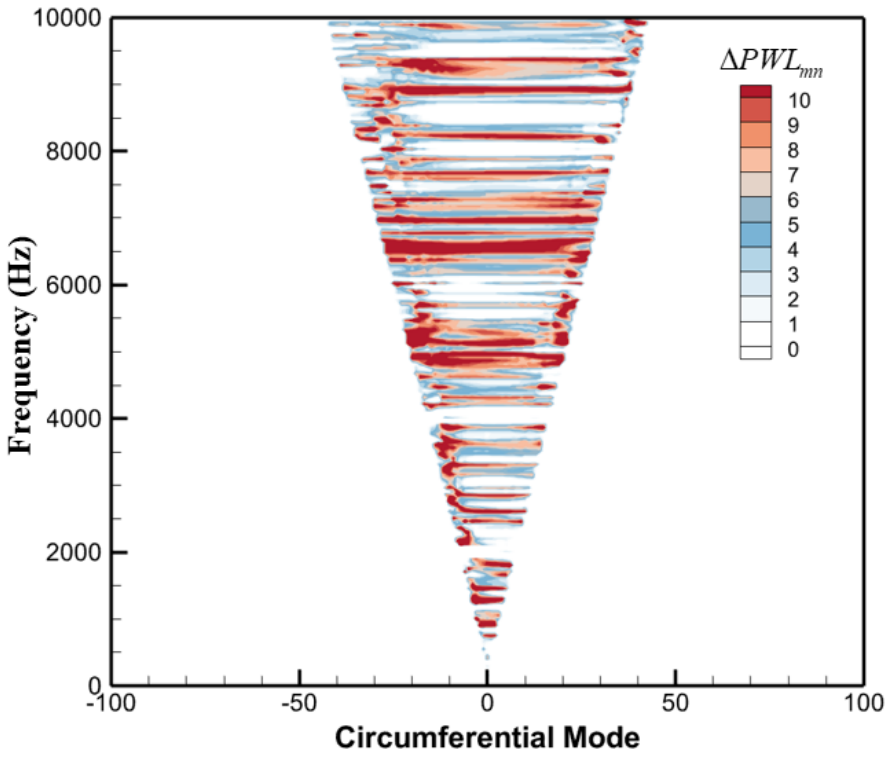

Figure 5. Modal PWL changes with Bionic R with frequencies ($\Delta PWL_{mn} = PWL_{mn,baseline} - PWL_{mn,bionic\ R}$).

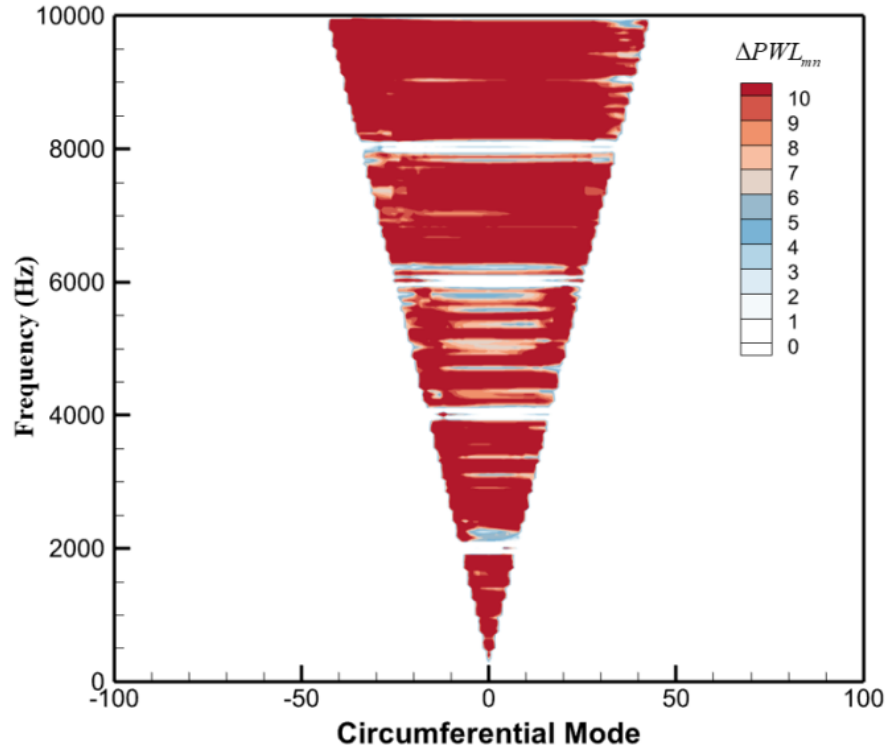

Figure 6. Modal PWL changes with Bionic S with frequencies ($\Delta PWL_{mn} = PWL_{mn,baseline} - PWL_{mn,bionic\ S}$).

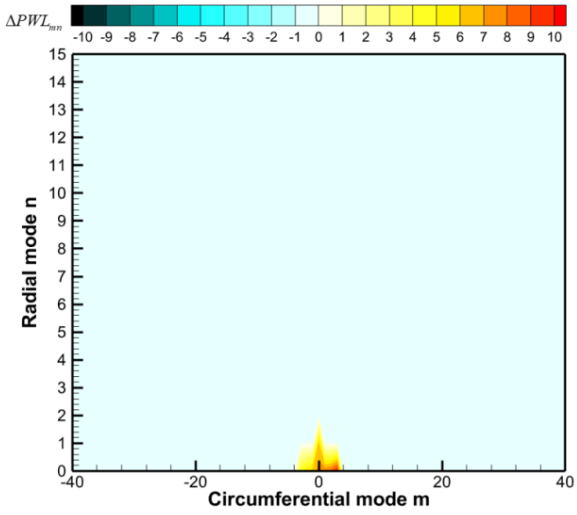
ΔPWL_{mn}
-10 -9 -8 -7 -6 -5 -4 -3 -2 -1 0 1 2 3 4 5 6 7 8 9 10
Radial mode n
Circumferential mode m

(a)

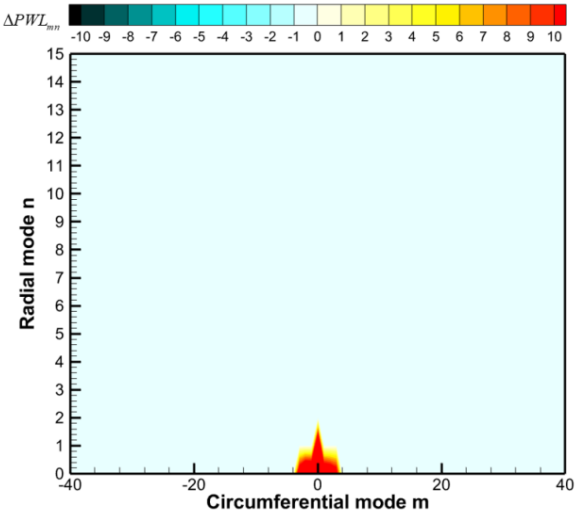
ΔPWL_{mn}
-10 -9 -8 -7 -6 -5 -4 -3 -2 -1 0 1 2 3 4 5 6 7 8 9 10
Radial mode n
Circumferential mode m

(b)

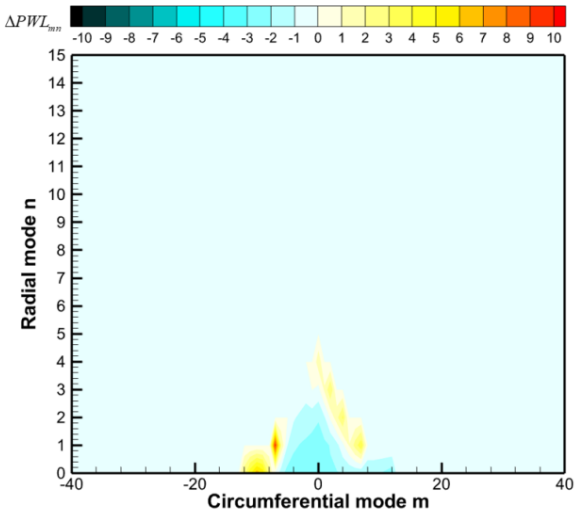
ΔPWL_{mn}
-10 -9 -8 -7 -6 -5 -4 -3 -2 -1 0 1 2 3 4 5 6 7 8 9 10
Radial mode n
Circumferential mode m

(c)

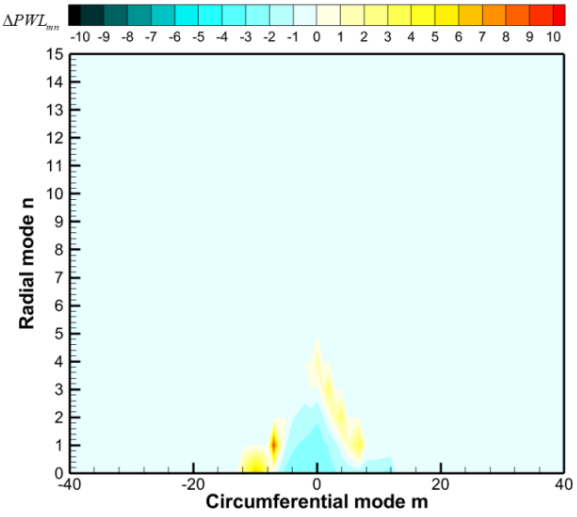
ΔPWL_{mn}
-10 -9 -8 -7 -6 -5 -4 -3 -2 -1 0 1 2 3 4 5 6 7 8 9 10
Radial mode n
Circumferential mode m

(d)

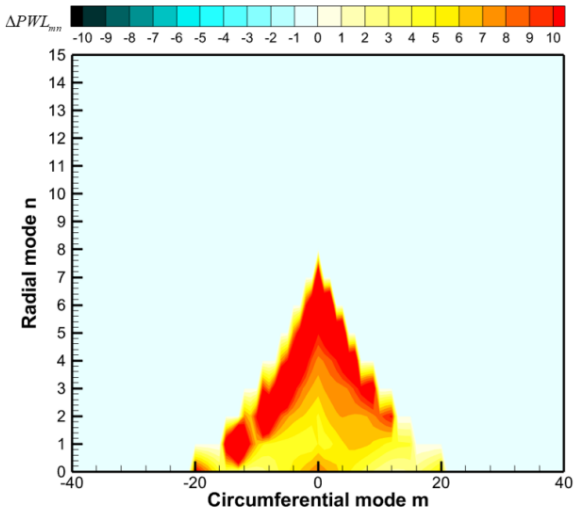
ΔPWL_{mn}
-10 -9 -8 -7 -6 -5 -4 -3 -2 -1 0 1 2 3 4 5 6 7 8 9 10
Radial mode n
Circumferential mode m

(e)

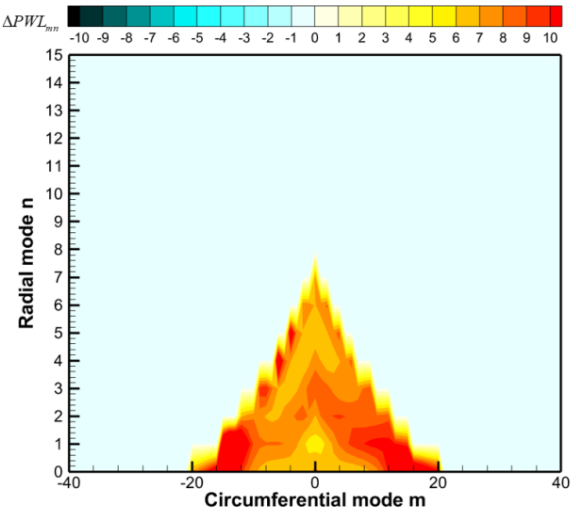
ΔPWL_{mn}
-10 -9 -8 -7 -6 -5 -4 -3 -2 -1 0 1 2 3 4 5 6 7 8 9 10
Radial mode n
Circumferential mode m

(f)

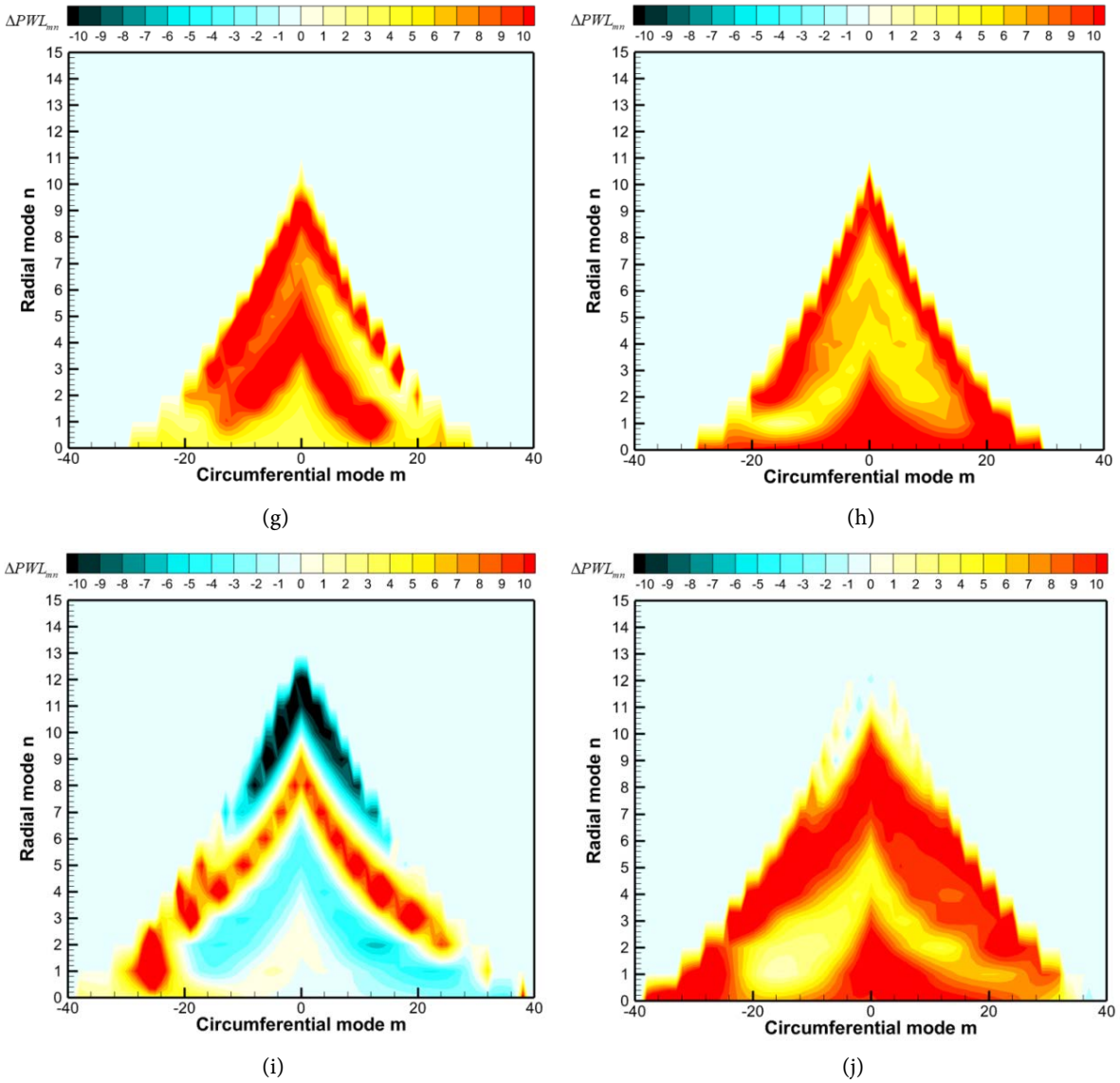

Figure 7. PWL changes of mode (m, n) at different frequencies ($\Delta PWL_{mn} = PWL_{mn,baseline} - PWL_{mn,bionic\ S}$). (a) 1000 Hz, Bionic R; (b) 1000 Hz, Bionic S; (c) 3000 Hz, Bionic R; (d) 3000 Hz, Bionic S; (e) 5000 Hz, Bionic R; (f) 5000 Hz, Bionic S; (g) 7000 Hz, Bionic R; (h) 7000 Hz, Bionic S; (i) 9000 Hz, Bionic R; (j) 9000 Hz, Bionic S.

different A/W on duct acoustic mode. However, it has found that serrated configurations have a significant impact on modes, and this influence has certain characteristics rather than being disordrly.

Figure 8 gives that PWL_{mn} distribution of different configurations at serval typical frequencies (1000 Hz, 5000 Hz and 9000 Hz). For the baseline, at 1000 Hz, the main duct modes are around m = 0, and are almost perfectly symmetric centered at m = 0. However, at 5000 Hz and 9000 Hz, the dominant duct modes move in positive m. Combined with **Figure 7**, it is demonstrated again that serration greatly make influence on the noise sources characteristics of duct modes.

Actually, the serration location at spanwise direction like only hub or shroud with serration and serration structure with more A/W needed to be further

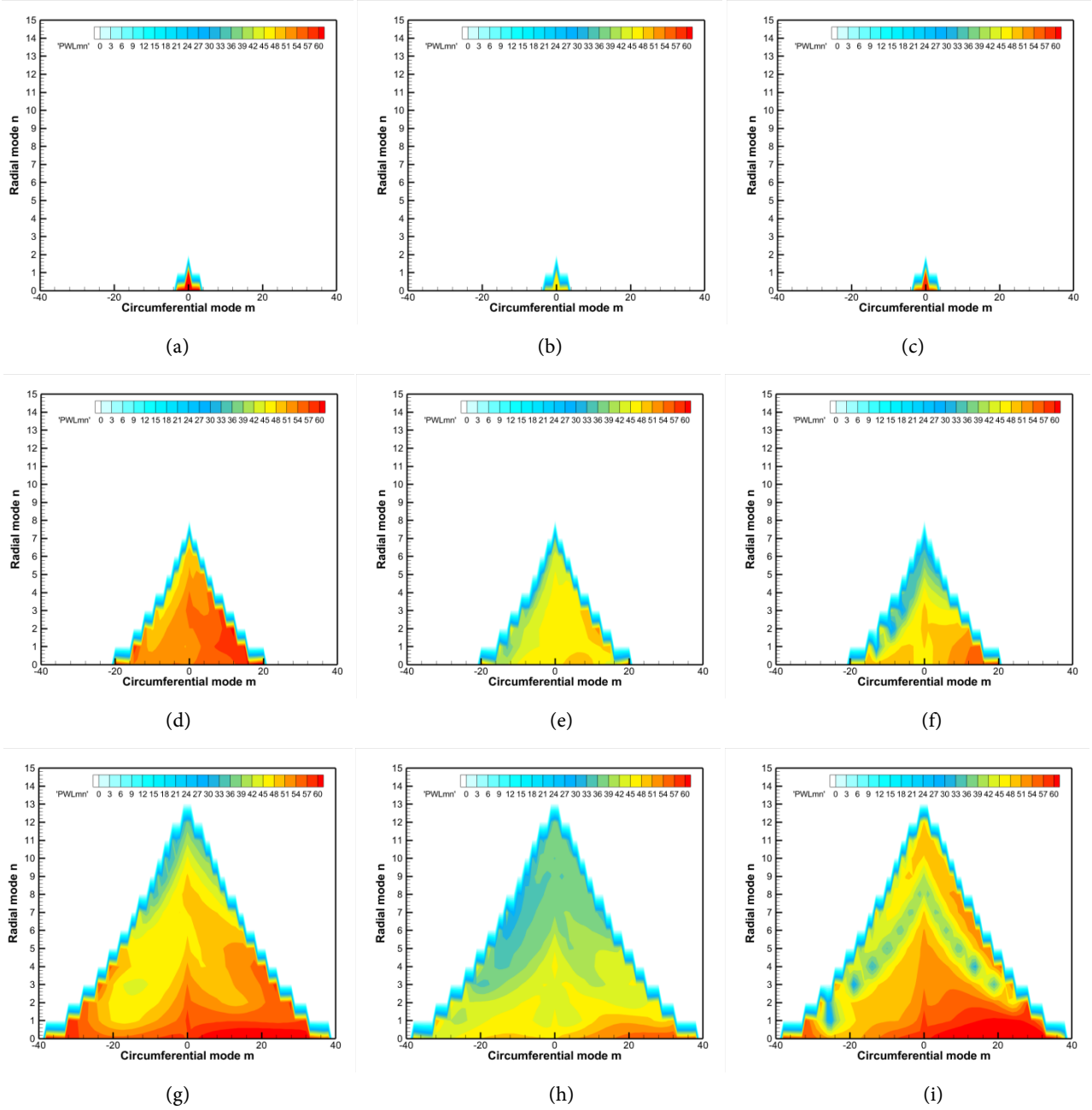

Figure 8. PWL_{mn} distribution of baseline and bionic configurations at serval frequencies. (a) 1000 Hz, Baseline; (b) 1000 Hz, Bionic S; (c) 1000 Hz, Bionic R; (d) 5000 Hz, Baseline; (e) 5000 Hz, Bionic S; (f) 5000 Hz, Bionic R; (g) 9000 Hz, Baseline; (h) 9000 Hz, Bionic S; (i) 9000 Hz, Bionic R.

studied to help master such mechanism and law in the next step.

6. Conclusions

Based on previous work [22], here further studied the effect of stator with serrated trailing-edge and rotor with serrated leading-edge on duct acoustic mode. First, both the acoustic modal source distribution and noise reduction gain at different modes of different frequencies show an approximately symmetric dis-

tribution, but this symmetry is not complete. Second, noise reduction didn't happen for all modes. At 9000 Hz, PWL of lots of modes (m, n) was no change and there are 10 dB increased in the range of circumferential mode −2 to 2 and radial mode 8 to 13. Third, the studies of the relation between bionics and mode are too "empty". There is no sufficient theory to support the mechanism and regularity of the research work but it is so significant. More works need to be done.

Nevertheless, this paper provides preliminary evidence that bionic configuration has the ability to control acoustic mode energy distribution of turbine interaction noise, and this has the potential to be one of technologies to break the existing bottlenecks of noise reduction dilemma.

Acknowledgements

The authors are grateful to Prof. Qiao Weiyang and Associate Prof. Chen Weijie for guiding and discussing. This study was co-supported by the National Science and Technology Major Project of China (No. 2017-Ⅱ-0008-0022), Aero Engine and Gas Turbine Basic Science Center (P2022-A-II-003-001, P2022-B-II-011-001) the National Natural Science Foundation of China (Nos. 52276038, 51936010, 52106056).

Conflicts of Interest

The authors declare no conflicts of interest regarding the publication of this paper.

References

[1] Moreau, S. (2019) Turbomachinery Noise Predictions: Present and Future. *Acoustics*, **1**, 92-116. https://doi.org/10.3390/acoustics1010008

[2] Radespiel, R. and Semaan, R. (2019) Fundamentals of High Lift for Future Civil Aircraft. 1th Edition, Braunschweig, Germany.

[3] Hughes, C. (2013) NASA Collaborative Research on the Ultra High Bypass Engine Cycle and Potential Benefits for Noise, Performance, and Emissions. Technical Memorandum TM-2013-216345; NASA: Washington, DC, USA.

[4] Hultgren, L.S. (2011) Emerging Importance of Turbine Noise. *International Journal of Aeroacoustics*, **10**, i-iv. https://doi.org/10.1260/1475-472X.10.1.i

[5] Nesbitt, E. (2011) Towards a Quieter Low Pressure Turbine: Design Characteristics and Prediction needs. *International Journal of Aeroacoustics*, **10**, 1-15. https://doi.org/10.1260/1475-472X.10.1.1

[6] Hu, Y.S., *et al.* (2022) Noise Reduction Mechanisms for Insert-Type Serrations of the NACA-0012 Airfoil. *Journal of Fluid Mechanics*, **941**. https://doi.org/10.1017/jfm.2022.337

[7] Singh, S.K., *et al.* (2022) On the Reductions of Airfoil Broadband Noise through Sinusoidal Trailing-Edge Serrations. *Journal of Aerospace Engineering*, **35**. http://dx.doi.org/10.1061/(ASCE)AS.1943-5525.0001386

[8] Singh, S.K. and Narayanan, S. (2023) Control of Airfoil Broadband Noise through Non-Uniform Sinusoidal Trailing-Edge Serrations. *Physics of Fluids*, **35**.

https://doi.org/10.1063/5.0133556

[9] Casalino, D., *et al.* (2019) Aeroacoustic Study of a Wavy Stator Leading Edge in a Realistic Fan/OGV Stage. *Journal of Sound and Vibration*, **442**, 138-154. https://doi.org/10.1016/j.jsv.2018.10.057

[10] Tong, F., *et al.* (2018) On the Study of Wavy Leading-Edge Vanes to Achieve Low Fan Interaction Noise. *Journal of Sound and Vibration*, **419**, 200-226. https://doi.org/10.1016/j.jsv.2018.01.017

[11] Cannard, M., *et al.* (2020) Physical Mechanisms and Performance of Slitted Leading-Edge Profiles for the Reduction of Broadband Aerofoil Interaction Noise. *Journal of Sound and Vibration*, **473**. https://doi.org/10.1016/j.jsv.2020.115214

[12] Kholodov, P. and Moreau, S. (2021) Optimization of Trailing-Edge Serrations with and without Slits for Broadband Noise Reduction. *Journal of Sound and Vibration*, **490**. https://doi.org/10.1016/j.jsv.2020.115736

[13] Ocker, C., *et al.* (2022) Aerodynamic and Aeroacoustic Properties of Axial Fan Blades with Slitted Leading Edges. *Acta Acustica*, **6**. https://doi.org/10.1016/j.jsv.2020.115736

[14] Bowen, L., *et al.* (2022) The Effect of Leading-Edge Porosity on Airfoil Turbulence Interaction Noise. *Journal of the Acoustical Society of America*, **152**, 1437-1448. https://doi.org/10.1121/10.0013703

[15] Palleja-Cabre, S., *et al.* (2022) Downstream Porosity for the Reduction of Turbulence-Aerofoil Interaction Noise. *Journal of Sound and Vibration*, **541**. https://doi.org/10.1016/j.jsv.2022.117324.

[16] Kangshen, X., Weijie, C., *et al.* (2022) Numerical Analysis on Sound Characteristics and Bionic Control of Turbine Tonal Noise. AIAA AVIATION 2022 Forum, June 27-July 1, Chicago, IL & Virtual. https://doi.org/10.2514/6.2022-3673.

[17] Tyler, J.M. and Sofrin, T.G. (1962) Axial Flow Compressor Noise Studies. *SAE Trans*, **70**, 309-332.

[18] Spalart, P.R., Jou, W.H., *et al.* (1997) Comments on the Feasibility of LES for Wings, and on a Hybrid RANS-LES Approach. Advances in DNS/LES, ed. C. Liu, Z. Liu, 137-147. Columbus, OH: Greyden Press.

[19] Spalart, P.R., Deck, S., *et al.* (2006) A New Version of Detached-Eddy Simulation, Resistant to Ambiguous Grid Densities. *Theoretical and Computational Fluid Dynamics*, **20**, 181-195.

[20] Shur, M.L., Spalart, P.R., *et al.* (2008) A Hybrid RANS-LES Approach with Delayed-DES and Wall-Modelled LES Capabilities. *International Journal of Heat and Fluid Flow*, **29**, 1638-1649.

[21] Goldstein, M.E. (1976) Aeroacoustics. Mc Graw-Hill: New York, NY, USA. https://doi.org/10.1017/S0022112077211256.

[22] Xiang, K.S., Chen, W.J., *et al.* (2023) Numerical Study of Stator Serrated Trailing-Edge on Control Turbine Broadband Noise. *Journal of Aerospace Power*. (in Chinese)